Neutron diffraction study of the tetragonal – monoclinic phase transition in $NdNbO_4$ and $NdTaO_4$

Matilde Saura-Múzquiz[1], Bryce G. Mullens[1], Helen E. Maynard-Casely[2] and Brendan J. Kennedy[1*]

[1] School of Chemistry, The University of Sydney, Sydney, New South Wales 2006, Australia

[2] Australian Nuclear Science and Technology Organisation, Lucas Heights, New South Wales 2234, Australia

[*] Corresponding Author: Brendan J. Kennedy (brendan.kennedy@sydney.edu.au)

Abstract

Phase transition and high-temperature properties of $NdNbO_4$ and $NdTaO_4$ were studied *in situ* using powder neutron diffraction methods. Both oxides undergo a reversible phase transition from a monoclinic $I2/a$ phase at low temperatures to a tetragonal $I4_1/a$ phase at high temperatures. The phase transition has been investigated through analysis of the spontaneous strains and symmetry distortion modes. Well below the transition temperature, T_c, the thermal evolution of the lattice parameters and symmetry modes suggest the transition is continuous, although a small discontinuity in both the spontaneous strains and symmetry distortion modes shows the transition is strictly first order. Analysis of the refined structures reveals that the Nb and Ta cations are best described as having a distorted 6-coordinate arrangement in the monoclinic structure, with four short and two long bonds. Breaking of the two long bonds at high temperatures, resulting in a transformation of the Nb(Ta) coordination to a regular tetrahedron, is believed to be responsible for the first order nature of the transition.

Introduction

The discovery and optimisation of materials capable of ionic conductivity is a critical endeavour in the transition to a low carbon economy. Orthoniobates and tantalates of the type $LnBO_4$ (*Ln* = lanthanoid; *B* = Nb or Ta) exhibit several technologically important properties including low thermal conductivity,[1] high temperature ionic conductivity,[2] remarkable chemical and radiation stability[3] and also hosts for laser materials.[4, 5] A number of the orthoniobates are ferroelastic materials that undergo reversible structural phase transitions. The ionic conductivity of these materials are of particular importance since structures containing tetrahedral moieties offer geometric flexibility that may enhance oxide ion conductivity.[6, 7] The $LnBO_4$ oxides may provide a means to develop solid oxide fuel cells that operate at modest temperatures.[2]

The crystal structure of the orthotantalates is largely determined by the ionic radius of the lanthanoid.[8, 9] The $LnTaO_4$ oxides containing the largest *Ln* cations (La-Pr) crystallize in either a nonpolar monoclinic space group $P2_1/c$, "*M*-$LaTaO_4$" or polar orthorhombic space group $Cmc2_1$, "*O*-$LaTaO_4$" structure depending on the synthetic conditions. Reducing the size of the *Ln* cation (Nd-Er) favours the formation of the monoclinic fergusonite $I2/a$ (a non-standard setting of $C2/c$, $Z = 4$) *M*-type structure, whereas the $LnTaO_4$ oxides containing still

smaller *Ln* cations (Tm-Lu) often display second monoclinic "*M*'-type" structure with space group $P2/c$. The room temperature structure of $NdTaO_4$, first reported by Keller[10] in 1962, was refined using powder neutron diffraction (PND) data by Marezio and co-workers in 1980.[11] The presence of the very heavy Ta cation (Z = 73) makes neutron diffraction indispensable for refining this structure, rather than relying on X-ray diffraction. This work revealed the existence of two long Ta-O contacts at 2.353(3) Å in addition to four much shorter (1.861(3) or 1.941(2) Å) bonds leading these workers to conclude that the Ta^{5+} cation has a distorted sixfold coordination. Tsunekawa and co-workers came to a similar conclusion from higher resolution PND data.[12] Earlier Stubican had reported that at temperatures above ~1600 K (1330 °C) $NdTaO_4$ undergoes a reversible phase transition from a monoclinic structure to the tetragonal scheelite-type structure.[13] The *I2/a* monoclinic structure is often described as being a distorted variant of the tetragonal scheelite ($CaWO_4$ space group $I4_1/a$, $Z = 4$) structure that contains isolated tetrahedra. Siqueira and Dias[14] reported that single-phase ceramic samples of $NdTaO_4$ can only be obtained by annealing at temperatures above 1473 K (1200°C). At lower temperatures a metastable tetragonal phase *T'* was observed, although details of this structure were not reported. The boundary between the various structures of the *Ln*TaO_4 orthotantalates can be altered by tuning the synthetic conditions, resulting in uncertainty and controversy in the literature. For example, Titov and co-workers showed that the $P2_1/c$ polymorph could be recovered from samples of *O*-type $NdTaO_4$ treated at 8GPa and 1000 °C.[15]

In comparison, the orthoniobates all exhibit the monoclinic fergusonite *M*-type structure at room temperature highlighting an unexpected difference between the two series.[8, 16] The ionic radii of Nb^{5+} and Ta^{5+} are generally considered to be identical,[17] as a consequence of the lanthanoid contraction, and their crystal chemistries are expected to be similar. The *M*-type orthoniobates are all ferroelastic materials that undergo reversible structural phase transitions at elevated temperatures to the scheelite structure.[18, 19] The application of pressure, as expected, appears to increase the monoclinic distortion of the orthoniobates and there is evidence for pressure induced phase transitions to other structures.[20, 21] In a series of studies of $LaNbO_4$, David and co-workers confirmed that the Nb^{5+} cations are tetrahedrally coordinated in the high temperature tetragonal structure, the Nb-O distance being 1.862(2) Å.[22] Marezio and co-workers [11] noted the presence of the long Nb-O contacts at 2.482(2) Å in $CeNbO_4$ but concluded that these should not be considered as bonds, although Tsunekawa concluded that these made a significant contribution to the bonding of the Nb cation.[12] Subsequently, most descriptions of the fergusonite structure are described as containing isolated BO_4 tetrahedra. The importance of the long contacts on the phase transition behaviour of the orthoniobates and tantalates remains unresolved.

Previous studies have described the $I2/a$ to $I4_1/a$ transformation in the orthoniobates as being continuous and second-order.[23, 24] There is, however, a substantial body of evidence showing that the two phases can co-exist at elevated temperatures.[25-27] Such behaviour is inconsistent with a continuous transition, suggesting that the $I2/a$ to $I4_1/a$ transformation may in fact be first order. Little is known about the transitions in the corresponding orthotantalates, other than they occur at higher temperatures.[28] The present work reports the results of variable temperature neutron diffraction studies of Nd*B*O_4 (*B* = Nb and Ta) that establish the temperature dependence of the long *B*-O bond with the aim of understanding the nature of the $I2/a$ to $I4_1/a$ phase transition.

Experimental

Polycrystalline $NdNbO_4$ and $NdTaO_4$ samples were prepared following a conventional solid-state synthesis method. The constituent oxides of each compound (Nd_2O_3 Sigma Aldrich 99.9%, Ta_2O_5 Aithaca Chemicals 99.99%, Nb_2O_5 Aithaca Chemicals 99.99%) were dried in a furnace at 1000 °C for 12 h to remove any potential water or carbon dioxide adsorbed by the powders. The corresponding oxides were then mixed in stoichiometric amounts and ground in an agate mortar with acetone until dry. The mixtures were transferred to alumina crucibles and annealed at 1000 °C for 12 h, after which they were re-ground in acetone until dry and pressed into a rod using a hydrostatic press for 2 minutes at 10 MPa followed by an additional 10 minutes at 20 MPa. The compacted rods were placed in alumina crucibles and annealed at 1200 °C for 18 h. This process (re-grinding in acetone and compacting) was repeated and the rods were re-annealed at 1400 °C for 36 h. Since none of the reactants are volatile under the synthesis conditions, we have assumed the products have their nominal stoichiometry.

Neutron powder diffraction experiments were performed with neutrons of wavelength 1.5413(1) Å, obtained with a single-crystal Ge [335] monochromator, on Wombat, the high intensity diffractometer at the OPAL reactor.[29] Polycrystalline samples of $NdNbO_4$ or $NdTaO_4$ were lightly ground and loaded into a 6 mm diameter vanadium can and affixed to a steel sample stick, with the whole assembly placed in an ILL-type high- vacuum furnace fitted with a Nb element that was operated at $< 10^{-4}$ Pa for the measurements. The temperature was measured using a thermocouple attached to the top of the sample holder. Variable temperature diffraction data were subsequently collected on both heating and cooling the sample. Data were collected for periods of five minutes with heating ramp rates of 1 K/min from RT to 500 °C and 0.5 K/min above this. The total number of data points collected during the heating ramp was 288 for $NdNbO_4$ and 427 for $NdTaO_4$. More details are given in the supplementary files.

The structures were refined by the Rietveld method as implemented in the program GSAS, [30, 31] The peak shapes were modelled using a pseudo-Voigt function, and the background was estimated by a 9-term shifted Chebyshev function. The background, scale factor, detector zero-point, lattice parameters, atomic coordinates and isotropic atomic displacement parameters were refined together with the peak profile parameters. The crystal structures were drawn using VESTA.[32] Where the monoclinic and tetragonal phases co-existed the peak profile parameters for the two phases were constrained to be equal in the Rietveld refinements. The atomic displacement parameters for the two different cations were constrained to be equal in both phases. The atomic positional and displacement parameters for the anions were unconstrained. Initially only the phase composition and lattice parameters were varied using the sequential refinement feature of GSAS. Where the phase composition was greater than 5 wt% the positional and atomic displacement parameters of the phase were refined. Where the sample contained less than 5 wt% these parameters were not refined. The refinements were undertaken starting from both the low temperature monoclinic region and the high temperature tetragonal region, for the data measured on both heating and cooling.

The bond valence of each ionic pair s_{ij} was calculated as: $s_{ij} = \exp[(R_0-R_{ij})/b]$ where R_0 and b are tabulated empirical parameters, equal to 1.92 (Ta), 1.911(Nb), 2.105(Nd), and 0.37 respectively. R_{ij} represents the $B(i)$–$O(j)$ bond length. The sum of the bond valence for each site i gives the BVS value $V_i = \sum_j s_{ij}$.[33, 34]

Results and Discussion

The structures of $NdNbO_4$ and $NdTaO_4$ between room temperature, 1000 and 1500 °C respectively were established by Rietveld refinement against powder neutron diffraction data. Figure 1 illustrates the neutron diffraction profiles of $NdNbO_4$ as the temperature is first increased from room temperature to 1000 °C and then decreased to 150 °C. This figure reveals the presence of both anisotropic thermal expansion of the monoclinic cell and the transformation to the tetragonal cell around 680 °C. The profile measured at room temperature was indexed to the monoclinic cell in space group $I2/a$ and the structure was successfully refined, see Figure 2, Tables 1 and 2. In the monoclinic structure the niobium cations are surrounded by four close oxygen ions, two O(1) and two O(2) arranged in a distorted tetrahedron, as illustrated in Figure 3. The average Nb-O distance of these four contacts is 1.88 Å corresponding to a Bond Valence Sum (BVS) of 4.39. There are another two oxygen ions with Nb-O distance of 2.486(2) Å. If these are considered to be bonded to the niobium atoms, the resulting BVS increases to 4.82. The BVS of the 8-coordinate Nd cation is 3.24. Thus, based on the BVS calculations it would appear that the Nb cation is six-coordinate with four short and two long bonds. The long Nb-O(1') distance found in $NdNbO_4$ is the same as that reported for $CeNbO_4$ (2.482Å) but is shorter than that seen in $LaNbO_4$ (2.542 Å).[12] The latter contributes 0.18 bvu (bond valence units) to the bonding of the Nb cation.

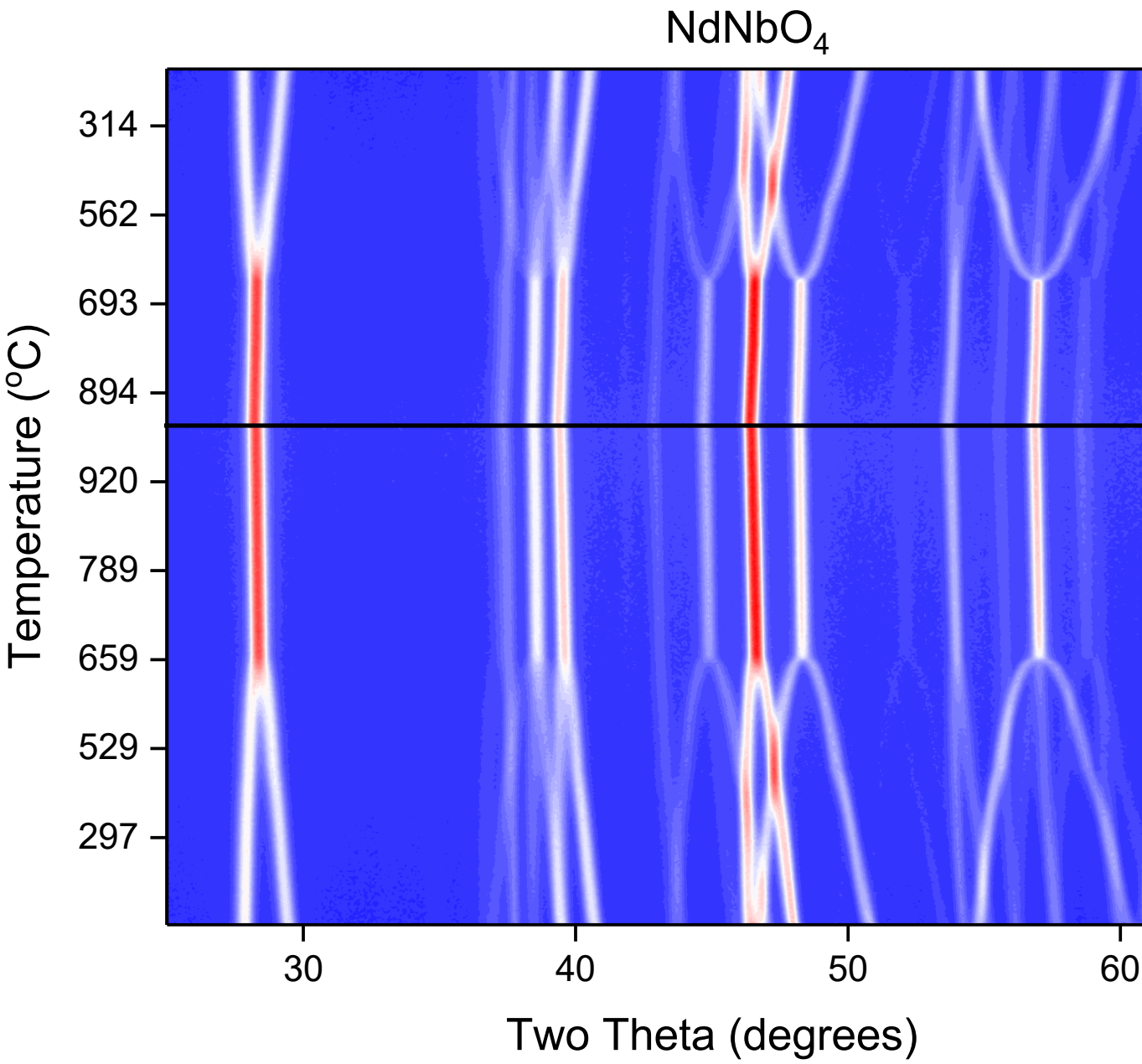

Figure 1. Portions of the temperature dependent neutron diffractograms for $NdNbO_4$ measured on heating to 1000 ºC and then re-cooling to 150 ºC. The *I*2/*a* to *I*4$_1$/*a* transition is apparent. The data were collected at 1.5413(1) Å.

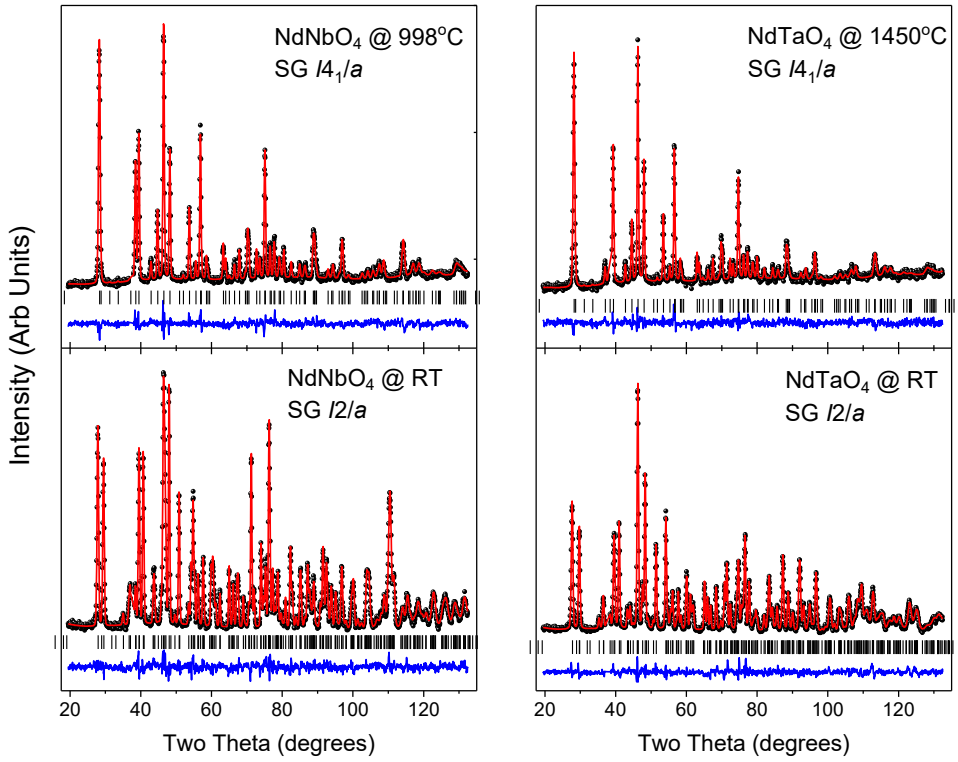

Figure 2. Rietveld refinement results for powder neutron diffraction data, measured at 1.5413(1) Å, $NdNbO_4$ and $NdTaO_4$. At room temperature the structures were refined in the monoclinic space group *I*2/*a* and at high temperatures the tetragonal space group $I4_1/a$ was used. In all cases the black spheres represent the observed data, the solid red line the fit to the measured profile. The lower blue line is the difference between the observed and calculated profiles. The vertical markers show the positions of the space group allowed Bragg reflections.

Table 1. Representative examples of the refined crystallographic data for $NdNbO_4$ and $NdTaO_4$ in the two identified space groups.

	$NdNbO_4$		$NdTaO_4$	
Temperature (ºC)	30	998	30	1450
Crystal System	Monoclinic	Tetragonal	Monoclinic	Tetragonal
Space group	*I*2/*a*	$I4_1/a$	*I*2/*a*	$I4_1/a$
Z	4	4	4	4
a (Å)	5.46272(18)	5.33980(22)	5.50402(22)	5.36144(29)
b (Å)	11.2666(4)	= *a*	11.2142(5)	= *a*
c (Å)	5.14029(18)	11.4765(6)	5.10419(21)	11.5203(8)
β (º)	94.5234(25)	90	95.7208(31)	90
V (Å^3)	315.381(19)	327.234(25)	313.479(22)	331.152(33)
R_{wp}	0.042	0.043	0.047	0.040
R_p	0.033	0.034	0.039	0.032
χ^2	1.38	1.62	1.67	1.23

Table 2. Representative examples of the refined Atomic positions and atomic displacement parameters of $NdNbO_4$ and $NdTaO_4$ in the two identified space groups.

$NdNbO_4$ Room Temperature SG *I*2/*a*					
Name	Wyckoff	*x*	*y*	*z*	Uiso*100 Å^2
Nd	4*e*	0.25	0.12050(20)	0	0.55(5)
Nb	4*e*	0.25	0.64488(19)	0	0.84(6)
O1	8*f*	0.0093(4)	0.71691(15)	0.2022(4)	1.01(5)
O2	8*f*	0.9021(4)	0.45647(18)	0.2420(4)	0.93(5)
$NdNbO_4$ 998 ºC SG *I*4$_1$/*a*					
Name	Wyckoff	*x*	*y*	*z*	Uiso*100 Å^2
Nd	4*a*	0	0.25	0.125	3.50(10)
Nb	4*b*	0	0.25	0.625	2.57(7)
O	16*f*	0.1645(3)	0.0009(5)	0.2120	4.43(6)
$NdTaO_4$ Room Temperature SG *I*2/*a*					
Name	Wyckoff	*x*	*y*	*z*	Uiso*100 Å^2
Nd	4*e*	0.25	0.11736(23)	0	0.46(5)
Ta	4*e*	0.25	0.65064(20)	0	0.56(7)
O1	8*f*	0.0147(4)	0.71803(19)	0.2180(5)	0.92(6)
O2	8*f*	0.9019(4)	0.45638(20)	0.2387(5)	0.89(5)
$NdNbO_4$ 1450 ºC SG *I*4$_1$/*a*					
Name	Wyckoff	*x*	*y*	*z*	Uiso*100 Å^2
Nd	4*a*	0	0.25	0.125	4.34(13)
Ta	4*b*	0	0.25	0.625	3.10(9)
O	16*f*	0.1652(4)	-0.0009(6)	0.2116(6)	5.75(9)

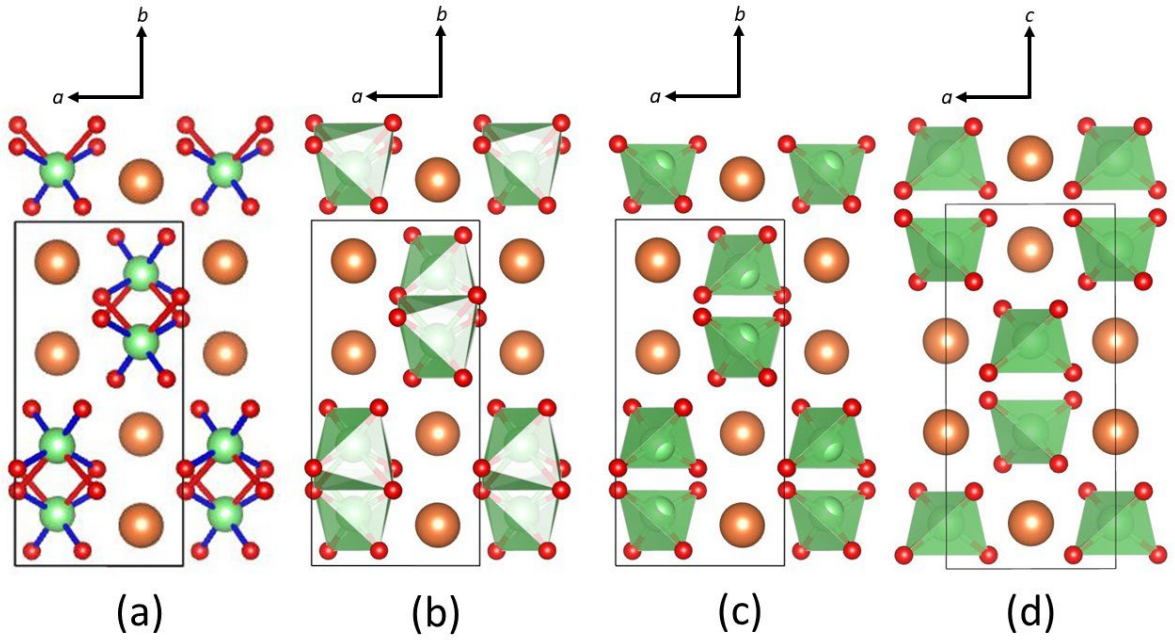

Figure 3. Representation of the Nd*B*O$_4$ structure. The gold and red spheres represent the Nd and O atoms respectively. (a) Ball and stick representation of the monoclinic *I*2/*a* structure showing the orientation of the four short (blue) and two long (red) bonds. In (b-d) the Nb(Ta) atoms are at the center of the green polyhedra. (b) The monoclinic *I*2/*a* structure illustrating the edge sharing distorted octahedra formed when including the long B-O(1') contact. (c) The monoclinic *I*2/*a* structure illustrating the isolated tetrahedra when the long B-O(1') contact is excluded. (d) the *I*4$_1$/*a* structure showing the tetrahedra.

The neutron profile of NdNbO$_4$ measured at 1000 °C, the highest temperature investigated, was successfully indexed to a tetragonal cell and the structure was refined using the scheelite model in space group *I*4$_1$/*a*.[35-37] In this high temperature tetragonal structure, there are four short Nb-O bonds with a distance of around 1.88 Å, corresponding to a BVS of 4.31 showing the Nb to be significantly under bonded, in the ideal case the BVS would be 5.0. There are four longer Nb-O contacts at 2.911(2) Å, which each contribute 0.07 bvu to the bond. Evidently, at high temperatures this contact is effectively non-bonding and it is appropriate to describe the coordination of the Nb as a distorted tetrahedron, although the Nb is significantly under bonded. The BVS for the Nd cation is 3.11.

The situation in NdTaO$_4$ is similar. The neutron diffraction profiles of NdTaO$_4$ illustrated in Figure 4 reveal the presence of a phase transition near 1200 °C and analysis of the data confirmed that this was between the monoclinic *I*2/*a* and tetragonal *I*4$_1$/*a* structures. Rietveld refinement using the data measured at room temperature provided accurate atomic coordinates for the anions. Considering only the four short Ta-O(1) 1.850(3) Å and Ta-O(2) 1.943(2) Å bonds, the BVS is an unrealistic 4.30, and this increases to 4.91when the two additional contacts at 2.355(3) Å are considered. These bond distances are in excellent agreement with the values reported in the early studies by Marezio and co-workers and Tsunekawa *et al.*,[11, 38] and show the Ta is effectively six coordinate with four short and two long bonds. The tetragonal structure, refined using the profile measured at 1500 °C has four short Ta-O bonds at a distance is 1.895(3) Å, corresponding to a BVS of 4.28. The longer Ta-O contact is 2.929(3) Å, which contributes only 0.07 bond valence units indicating that this contact cannot be considered as a bond. It is, of course, possible that the tabulated value of R_0 (1.92) for 4-coordinate Ta^V is incorrect when a value of 1.975 yields a BVS of 5.0. The BVS of the 8-coordinate Nd cation in NdTaO$_4$ at room temperature is 3.24.

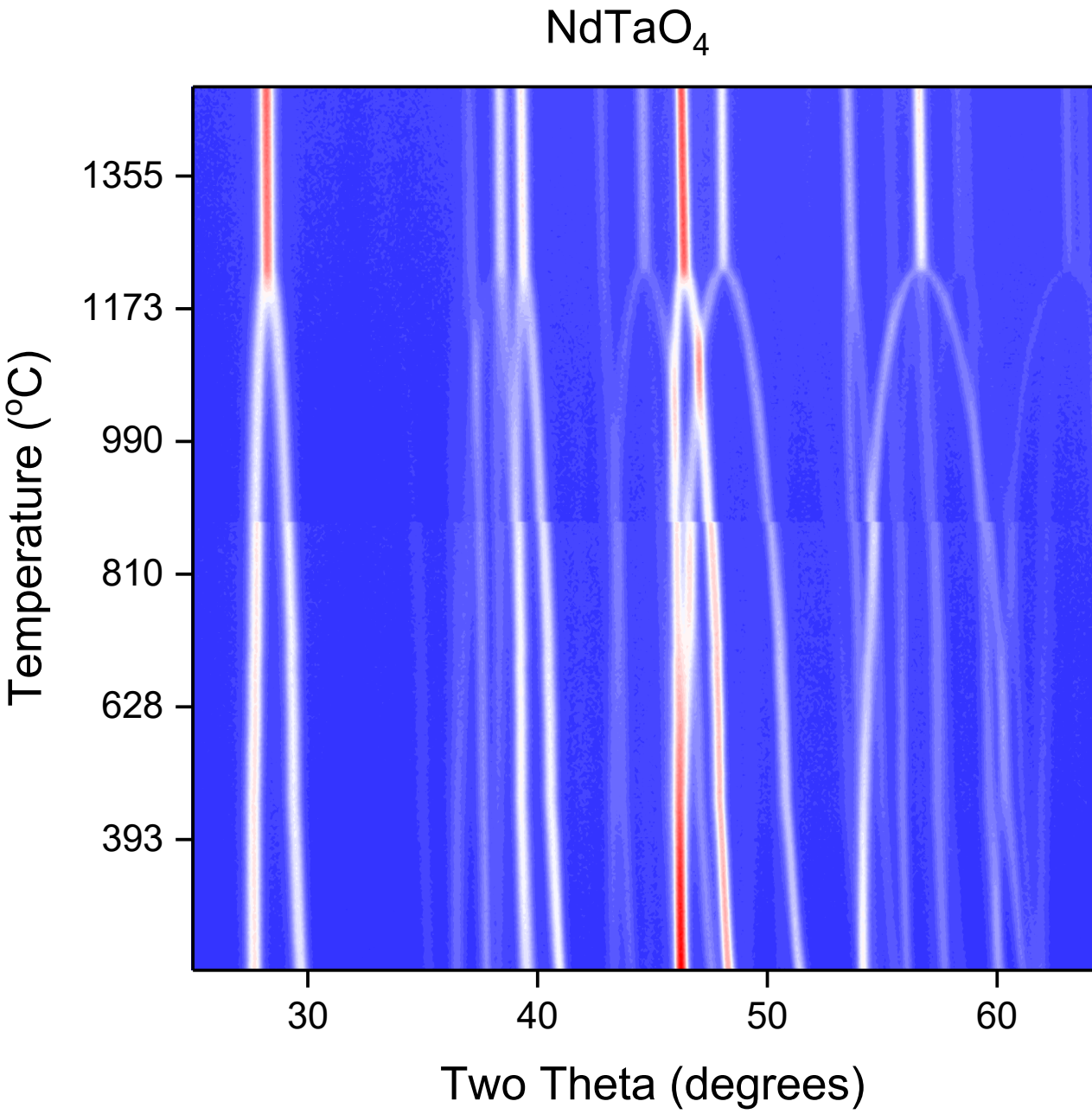

Figure 4. Portions of the temperature dependent neutron diffractograms (λ = 1.5413(1) Å) for $NdTaO_4$ measured on heating to 1500 ºC. The discontinuity near 900 ºC is an experimental artefact resulting from realignment of the sample.

The temperature dependence of the refined lattice parameters for $NdNbO_4$ and $NdTaO_4$ are shown in Figure 5. This figure highlights the anisotropic expansion of the monoclinic cell with the monoclinic *a*-parameter decreasing as the temperature increases whilst the monoclinic *c*-parameter increases, the two become equal at the transition to the

tetragonal structure. This transition is also revealed in the temperature dependence of the monoclinic β angle that is symmetry constrained to be 90º in the tetragonal phase. The unit cell volume increases approximately linearly in both the monoclinic and tetragonal phases, there being a notable change in the rate of expansion at the transition. The linear thermal expansion of the monoclinic phase is greater than that of the tetragonal phase for both $NdNbO_4$ and $NdTaO_4$, as shown in Figure 5 and Figure 6. The linear thermal expansion coefficient (α) was calculated as $\alpha = \frac{\Delta V}{V_i \Delta T}$, where V_i is the initial unit cell volume, ΔV is the change in unit cell volume over the corresponding temperature range ΔT. For the monoclinic phase of $NdNbO_4$ α was 4.5 x 10^{-5} Å K^{-1} and for $NdTaO_4$ it was 3.6 10^{-5} Å K^{-1}. The corresponding values in the tetragonal phase were 2.7 and 3.0 x 10^{-5} Å K^{-1} respectively. These observations are consistent with previous studies of ABO_4 oxides that display a temperature-induced $I2/a$ to $I4_1/a$ transition, including the recent work of Sarin,[26] and Arulnesan.[16]

Although there is no obvious discontinuity in the lattice parameters across the $I2/a$ to $I4_1/a$ transition suggesting the transition is continuous (second order or tricritical) Ning and co-workers noted that crystals of $NdTaO_4$ grown using the Czochralski method cracked along the [010] plane.[5] This can be possibly explained by anisotropic thermal expansion or it may indicate that the transition is first order. We will return to this point below.

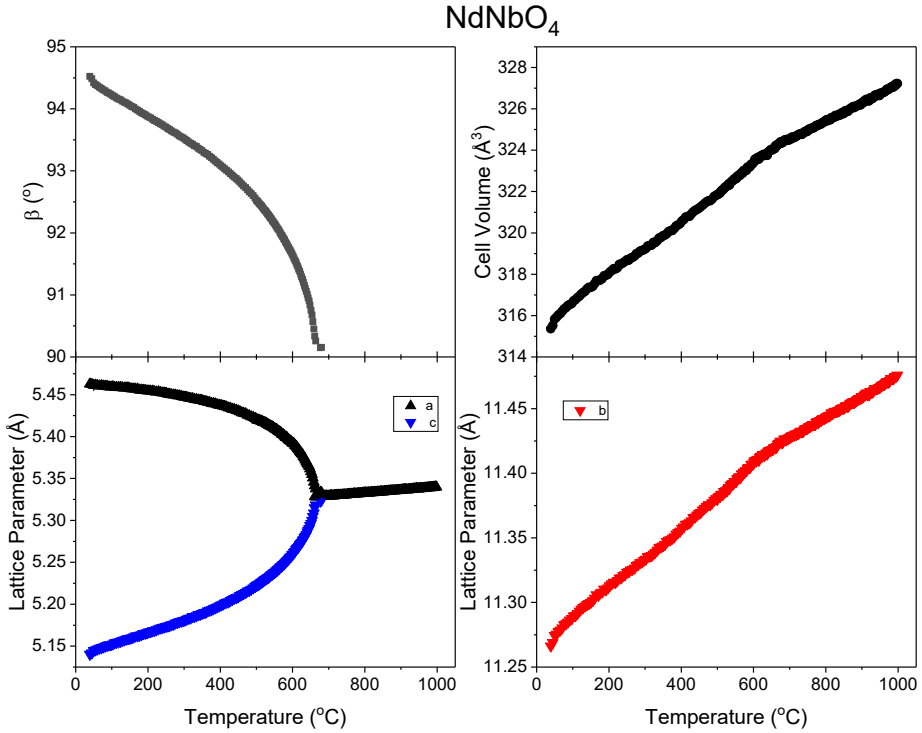

Figure 5(a). Temperature dependence of the unit cell parameters for $NdNbO_4$ obtained by Rietveld refinement against PND data. The data were collected as the sample was heated from room temperature to 1000 ºC. The error bars are smaller than the symbol size.

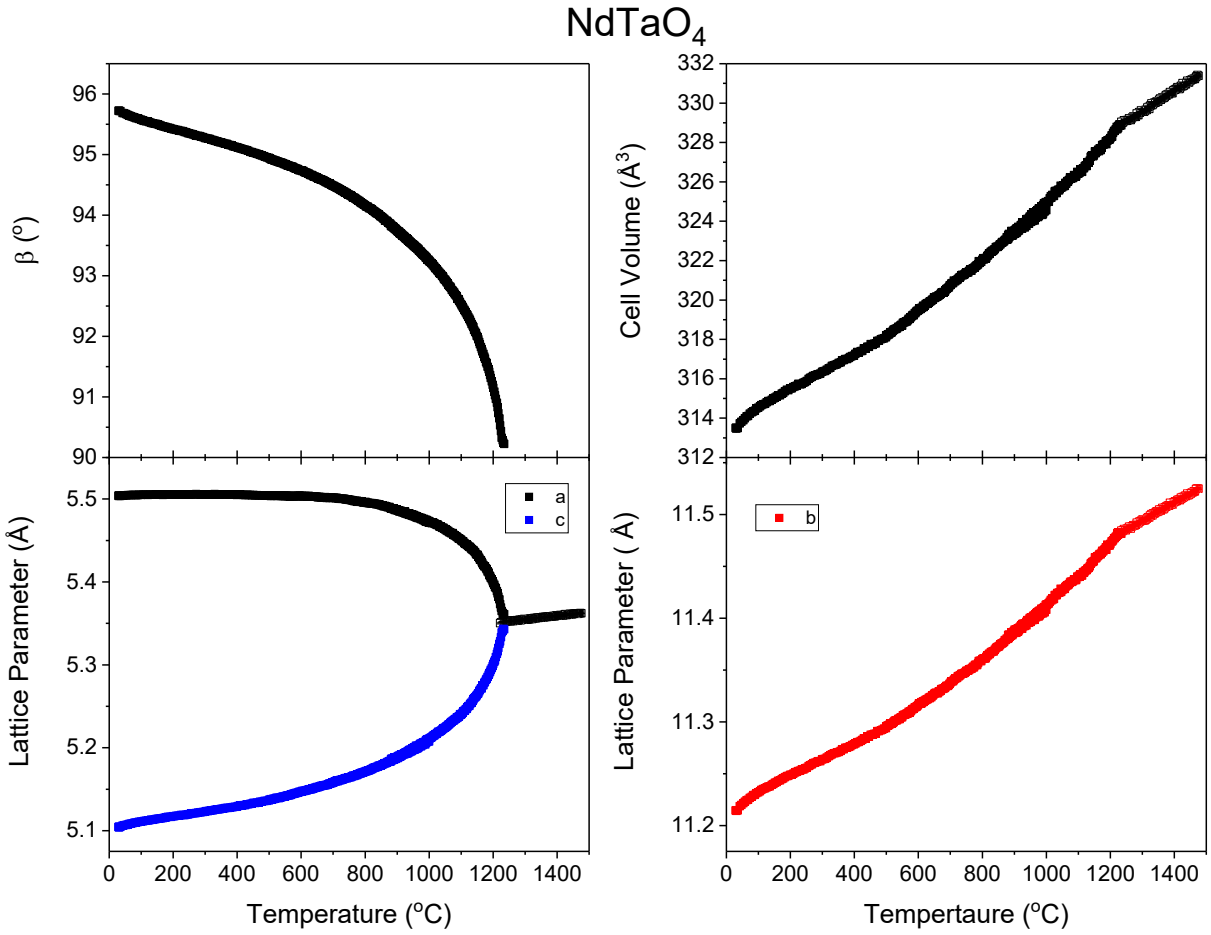

Figure 5(b). Temperature dependence of the unit cell parameters for $NdTaO_4$ obtained by Rietveld refinement against PND data. The data were collected as the sample was heated from room temperature to 1450 ºC. The error bars are smaller than the symbol size.

The temperature dependence of the *B*-O distances for both studied oxides are illustrated in Figure 6. The two short *B*-O distances in the monoclinic structure are symmetry constrained to the equal in the tetragonal structure. The long *B*-O distance shows an exponential-like increase with temperature in the monoclinic structure that abruptly stops at the transition to the tetragonal structure. As noted above, in the tetragonal structure the long *B*-O contacts are effectively non-bonding and the changes in the bond distances are indicative of a change from a distorted octahedral to regular tetrahedral environment. Figure 6 also illustrates the temperature dependence of the bond valence contributions for the three *B*-O distances identified above. In calculating these a temperature dependent bond valence parameters R_0^T,

defined as $R_0^T = R_0 + \left(\frac{dR}{dT}\right)\Delta T$ was used where $(dR/dT) = 9 \times 10^{-6}$ ÅK^{-1} and ΔT is the temperature difference from 298 K as described by Brown *et al.*[39] For both compounds the contribution of the long *B*-O(1') is strongly temperature dependent, whereas the contributions from the two shorter *B*-O(1) and *B*-O(2) distances are only weakly temperature dependent. Their behaviour mirrors the bond distances and highlights the greater contribution of the long *B*-O(1') bond in the Ta compound, which may be the cause of the higher transition temperature in the Ta compound. Jacquet *et al*. observed that, as also found in the current Nd*B*O_4 oxides, the NbO_6 polyhedra were more distorted than the TaO_6 polyhedra in Li_3BO_4 (*B* = Ru, Nb, Sb and Ta).[40] They ascribed this different to a second-order Jahn-Teller effect. Recent DFT calculations on the related pair of oxides, $HoNbO_4$ and $HoTaO_4$ have revealed differences in the charge delocalisation between the Nb and Ta oxides and such changes in covalency may also impact the transition temperature.[41] Shimakawa *et al*. showed that increasing the Nb content in $SrBi_2(Ta_{1-x}Nb_x)_2O_9$ resulted in an increase in the ferroelectric Curie temperature. These authors concluded that since the Nb 4*d* orbitals are less extended than the corresponding Ta 5*d* orbitals, its bonding will be more covalent driving the change in propoerties.[42]

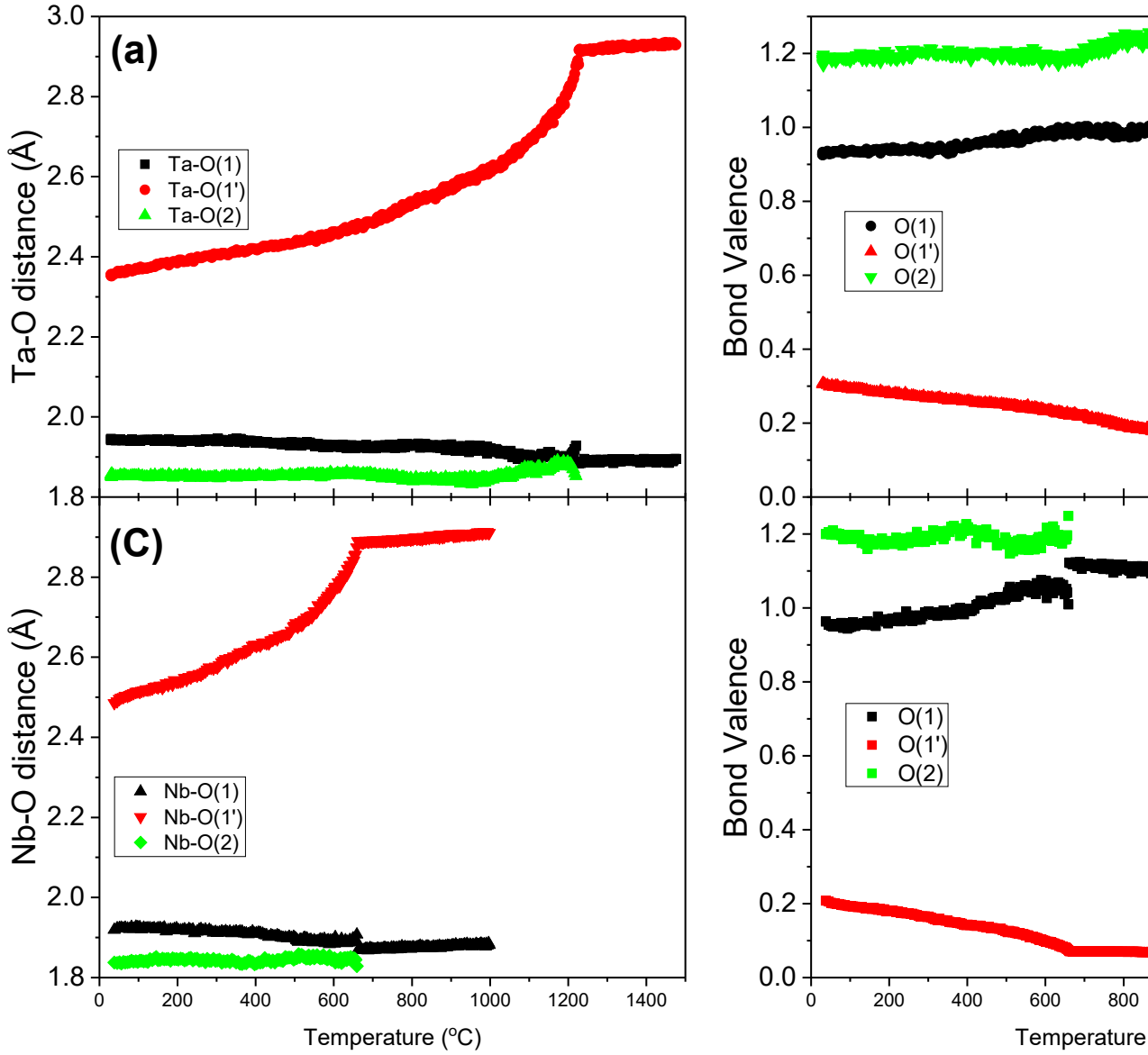

Figure 6. Temperature dependence of (a) the Ta-O bonds and (b) bond valence contributions for $NdTaO_4$ along with (c) the Nb-O bonds and (d) bond valence contributions for $NdNbO_4$ as obtained from Rietveld refinements against PND data.

Sarin *et al.*[26] stated in their recent synchrotron X-ray diffraction study of the *I*2/*a* to *I*4$_1$/*a* transition in the three orthoniobates $YNbO_4$, $LaNbO_4$, and $DyNbO_4$ that "*the bond valence analysis was inconclusive"* when considering the tetragonal to monoclinic transition associated with the change from tetrahedral (NbO_4) toward distorted octahedral (NbO_6)

coordination around the niobium ion. We contend that the current analysis, based on neutron diffraction data that is more sensitive to the more sensitive to the anion positions and hence the *B*-O bond lengths, unequivocally shows that such a change does indeed occur. Consequently, we conclude that it is more appropriate to describe the *I*2/*a* to *I*4$_1$/*a* transition as reconstructive, since it involves the formal breaking of a bond, than displacive that does not involve bond breaking.

We now turn our attention to the nature of the phase transition, in light of the above discussion that seems to indicate that the transition may, in fact, be first order rather than continuous. The fergusonite structure is typically described as a distorted and compressed version of the scheelite structure and can be derived from the high symmetry aristotype by significant displacement of the anions and a distortion of the cation matrix. Landau theory has previously been used to analyze the fergusonite-scheelite transition, including the pressure induced transition in scheelite ($CaWO_4$) itself. [43] According to the Landau theory of phase transitions, the excess free energy due to the transition in a single domain is:[44, 45]

$$G = \frac{A}{2}(T - T_c)Q^2 + \frac{B}{4}Q^4 + \frac{C}{6}Q^6 + \cdots. \qquad (1)$$

When *A*, *B* and *C* are all positive, this leads to a continuous phase transition at T_c. In many cases either *B* or *C* is sufficiently small, relative to the other, to be neglected leading to either second order behaviour where the order parameter $Q \propto (T_c - T)^{\frac{1}{2}}$ or tricritical behaviour $Q \propto (T_c - T)^{\frac{1}{4}}$. If both the *B* and *C* prefactors are significant, then more complex temperature dependence of the order parameter will occur. [45]

Schlenker concluded that the spontaneous strain calculated from the lattice parameter values can be used as the order parameter *Q* in the Landau theory, since the displacement of the atoms from the equivalent positions of the parent phase give rise to spontaneous strains.[46, 47]

The strain components are calculated as:

$$\varepsilon_{11} = \frac{c_M \sin\beta_M}{a_0} - 1$$

$$\varepsilon_{22} = \frac{a_M}{a_0} - 1$$

$$\varepsilon_{33} = \frac{b_M}{c_0} - 1$$

$$\varepsilon_{12} = \varepsilon_{21} = -\frac{c_M \cos\beta_M}{2a_0}$$

where a_0, b_0 and c_0 are the equivalent tetragonal lattice parameters, extrapolated from the strain free high symmetry phase. To enable a reasonable estimate of these values data were collected well above the transition temperature.

With $\varepsilon_{11}^s = \frac{1}{2}(\varepsilon_{11} - \varepsilon_{22})$ and $\varepsilon_{12}^s = \varepsilon_{12}$, the magnitude of the spontaneous strain $(\varepsilon^s)^2$ is given as

$$(\varepsilon^s)^2 = 2[\varepsilon_{11}^s)^2 + \varepsilon_{12}^s)^2].$$

The temperature dependence of the spontaneous strains is illustrated in Figure 7. Attempts to fit these with η = ½ or ¼ corresponding to a second order or tricritical transition were unsuccessful. Rather least squares fitting to the general expression:

$$\varepsilon^s = A(T_c - T)^\eta$$

showed that for $NdNbO_4$ η = 0.398 with T_c = 660 ºC and for $NdTaO_4$ η = 0.314 with T_c = 1217ºC. Evidently the pre-factor terms *B* and *C* of the Landau expression are both significant for this pair of oxides.[45]

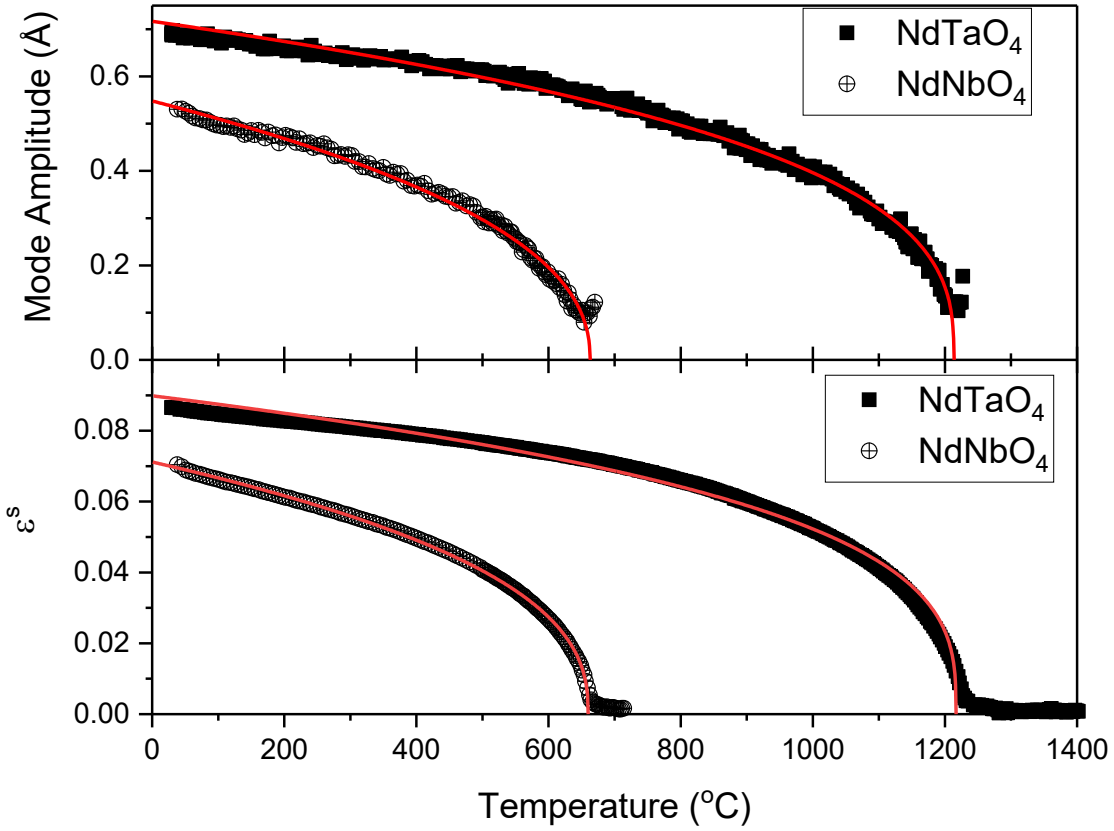

Figure 7. Temperature dependence of the spontaneous strains ε^s, calculated from the refined lattice parameters and the amplitude of the Γ_2^+. The solid lines are the fit to the expression $fn = A(T_c - T)^\eta$ with the fit parameters given in the text.

Whilst the spontaneous strains derived from the lattice parameters provide a convenient order parameter, it is pertinent to also consider the displacement modes of the low symmetry daughter structure, allowed by irreducible representation (*iirep*), of the higher symmetry aristotype. The distortion modes characteristic of the *I*2/*a* structure, relative to the *I*4$_1$/*a* scheelite were explored using the AMPLIMODES software.[48] Two modes, designated by the *irreps* Γ_1^+ and Γ_2^+, were identified, where the Γ_2^+ is the primary mode, that should act as

the order parameter for the phase transition. As discussed recently by Auckett and co-workers,[49] the Γ_2^+ mode causes in-plane displacement of the oxygen atoms resulting in twisting of the BO$_4$ polyhedra about the scheelite c-axis as well as displacements of the cations from their equivalent high symmetry (tetragonal scheelite) positions, this is illustrated in Figure 8. The displacements of the B-type cations are in the opposite sense along the c-axis and in alternate layers. Figure 8(b) highlights the rotation of the BO$_4$ polyhedra around the Nd atoms.

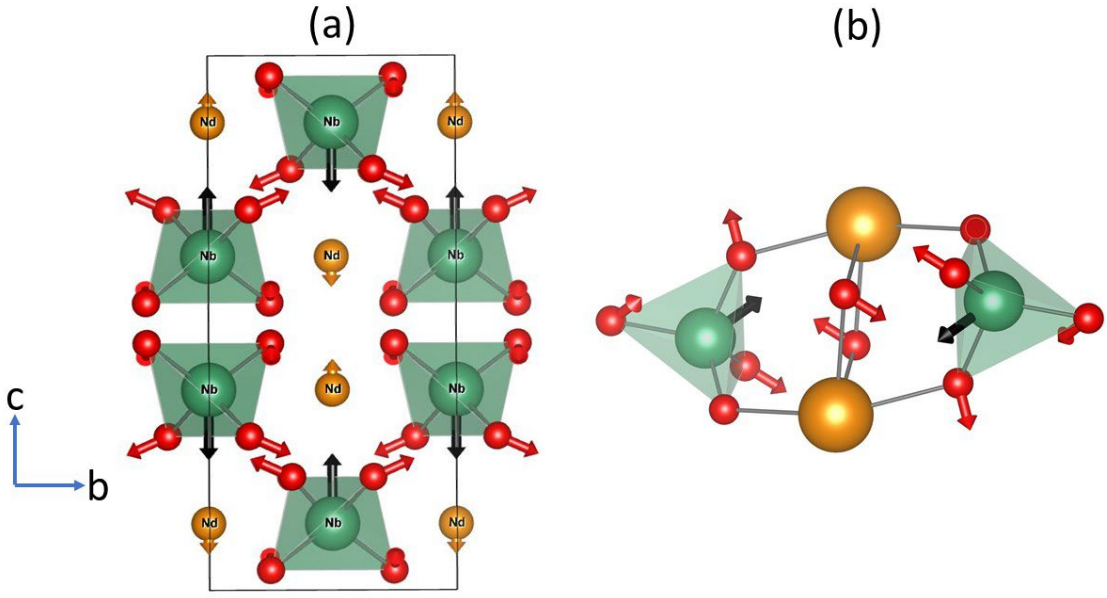

Figure 8. Representation of the atomic displacements in NdBO$_4$ (B = Nb, Ta) resulting from the Γ_2^+ modes. In both cases the small red spheres represent the oxygen anions, with the relative magnitude of their displacements illustrated by the red atoms. The larger green spheres, at the centre of BO$_4$ tetrahedra of the high symmetry $I4_1/a$ structure, represent the B-type cation with their relative displacements illustrated by the black arrows. The gold spheres represent the Nd cations. The relative displacement of these have been multiplied by 3 in (a) and are too small to be apparent in (b).

AMPLIMODES was then used to derive mode amplitudes from each refinement and the thermal evolution of the Γ_2^+ modes are given in Figure 7. The temperature dependence of the Γ_2^+ was analysed using the general expression $\Gamma = A(T_c - T)^{\eta}$ yielding for NdNbO$_4$ η = 0.348 with T_c = 660 ºC and for NdTaO$_4$ η = 0.348 with T_c = 1218 ºC. These values are in excellent agreement with the values deduced from analysis using the spontaneous strains. Indeed, plots of Γ_2^+ vs ε^s for both oxides are linear, see supplementary files. That both analysis show η is significantly different to ½ or 1/4 demonstrates that transition is neither second order or tricritical.[45] It is tempting to speculate that the progressive weakening of the long B-O(1) bond plays an important role in this behaviour. Hayward and Salje concluded that elastic strains associated with distortion of the TiO$_6$ in SrTiO$_3$ play a significant role in modifying the thermodynamic characteristic of the cubic to tetragonal transition.[45] Irrespective of the importance of the long B-O(1') contact in satisfying the bonding requirements of the pentavalent cation there is significant deformation of the BO$_6$ polyhedra that impacts the transition.

Figure 7 reveals discrepancies between the observed and calculated strains and distortion modes just below the transition to the monoclinic phase. These small discontinuities may simply be experimental artifacts reflecting the peak shape resolution of the diffractometer employed in this work or they may indicate that the transition is first order. In their earlier synchrotron XRD study of $NdNbO_4$, Sarin *et al.* reported the presence of a two- phase region around the $I2/a$ to $I4_1/a$ transition and postulated that this was a consequence of either the presence of a range of particle sizes in the sample, where the surface energy of the smaller sized particles alters the relative stability of the two structures, or there is coupling between the order parameter and the residual strains in individual crystallites.[26] Arulnesan and co-workers in their studies of related $LnNbO_4$ oxides also noted the presence of the co-existence of the $I2/a$ to $I4_1/a$ phases over a relatively wide temperature range. [16] Phase coexistence and hysteretic behaviour has been observed in related systems showing that the $I2/a$ to $I4_1/a$ phase transition is first order. However, if the energy barrier between the two states is sufficiently small, the transition can mimic a continuous transition. Auckett *et al.* estimated the energy barrier between the two phases in $LaNbO_4$ to be ~ 0.207 eV per unit cell, [49] and this appears to be small enough for the transition to appear to be continuous as judged by the evolution in the unit cell parameters.[24, 25, 28] Although first order transitions often have an associated volume discontinuity, this is not always observed as evidenced from the high resolution neutron diffraction study of the first order $I4/mcm$ to *Imma* transition in the perovskite $SrZrO_3$.[50]

Scrutiny of the PND profiles in the region of the $I2/a$ to $I4_1/a$ transition did not reveal any obvious evidence of the co-existence of the two phases for $NdNbO_4$ or $NdTaO_4$. We did, however, notice a decrease in quality of the fits across the transition as evident from the various measures of fit. For example, in $NdNbO_4$ χ^2 increased from 1.51 at 662 ºC to 1.60 at 688 ºC before decreasing again to 1.56 at 714 ºC. Consequently, the patterns measured between 620 and 720 ºC were analysed using a two phase $I2/a + I4_1/a$ model and the temperature dependence of the relative abundance of each of these is shown in Figure 9. This reveals a systematic increase in the amount of the tetragonal phase as the temperature was increased from ~ 650 to 670 ºC, as well as an evident hysteretic behaviour. The co-existence of the two phases together with the hysteresis shows the transition cannot be continuous (second order or tricritical). A feature of Figure 9 is the different rate of the transformation upon heating and cooling, the co-existence of the two phases is much less upon cooling. It appears that the transition in $NdNbO_4$ is fact first order, although well below the transition temperature ~ 650 ºC the transition is quasi-continuous and can be treated using Landau theory albeit with an atypical value of η. Similar results were obtained for $NaTaO_4$ and these are shown in the supplementary files.

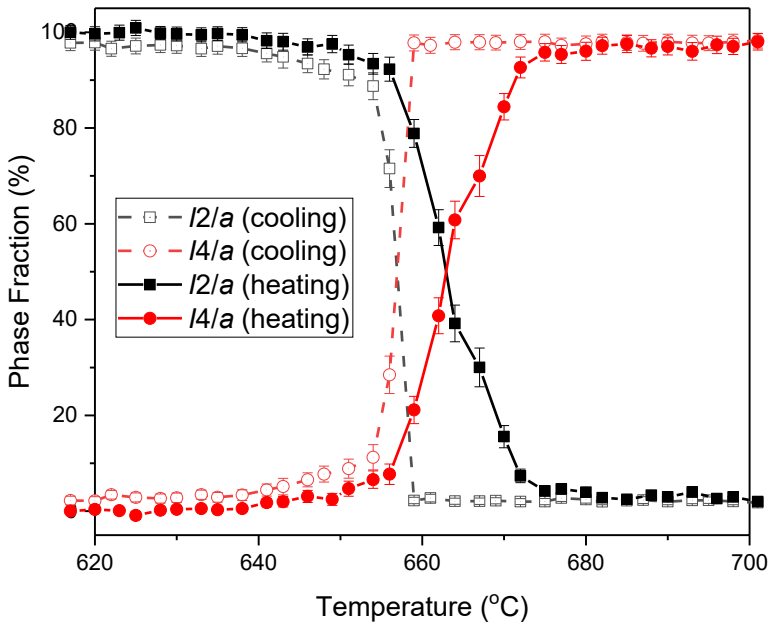

Figure 9. Temperature dependence of the tetragonal and monoclinic phase fractions in $NdNbO_4$ upon heating and cooling. The observed hysteresis and phase coexistence is suggestive of a first order transition. Where not apparent the esds are smaller than the symbols. The corresponding plot for $NdTaO_4$ is given in the supplementary files.

Finally it is pertinent to comment on the potential impact, if any, of the long B-O(1') bond on the oxide ion conductivity of these types of materials. The flexibility of the BO_n polyhedral to both deformation and rotation is believed to be important for oxide ion mobility.[7] The presence of oxygen vacancies in $La_{1-x}Ba_xGaO_{4-0.5x}$ results in the formation of corner sharing Ga_2O_7 units and oxygen vacancies migrating by means of continuous breaking and reformation of Ga_2O_7 dimers enabled by the rotation and deformation of the GaO_4 units.[7] The underbonding of the Nb(Ta) cations in the current scheelite -type oxides strongly argues against the involvement of three coordinate intermediates, as would occur if oxygen vacancies played a critical role in the oxygen ion conductivity. This points to the importance of oxygen interstitials. Ferrara and co-workers concluded, based on DFT calculations, that a number of interstitial sites are potentially accessible in scheelites and they identified an 8*e* site at 0 0 $z \sim 0.335$ (in setting #2 of SG 88) of particular interest.[51] This site is ~ 2.4 Å from the Nb(Ta) cations, a distance that is comparable to the long B-O(1') distance revealed in the current PND study of $NdNbO_4$ and $NdTaO_4$. Occupancy of this site would alleviate some of the underbonding of the *B*-site cations in the tetragonal structure.

Conclusions

In situ powder neutron diffraction measurements of $NdNbO_4$ and $NdTaO_4$ show that both oxides undergo a reversible monoclinic $I2/a$ to tetragonal $I4_1/a$ phase transition at high temperatures, ~ 660 and 1217 ºC respectively. In both cases the two phases co-existed over a small temperature range and the transitions showed hysteretic behaviour demonstrating that

they are a first order transition. Bond Valence Sum analysis of the refined structures reveals that the Nb and Ta cations are best described as having a distorted 6-coordinate arrangement in the monoclinic structure, with four short and two long bonds. Breaking of the two long bonds at high temperatures, resulting in a transformation of the Nb(Ta) coordination to a regular tetrahedron, is believed to be responsible for the first order nature of the transition. It was possible to analyse the spontaneous strains and symmetry distortion modes under the framework of Landau theory below the transition temperature, despite the transition being first order. Such analysis resulted in atypical values of η when fitted to an expression of the type $A(T_c - T)^{\eta}$, presumably as a consequence of the coupling between the twisting of the BO_6 groups described by the Γ_2^+ mode and the change in the bonding within the BO_6 polyhedra. Both the Nb and Ta cations are appreciably underbonded in the high temperature tetragonal structure, which may facilitate the occupancy of a nearby interstitial site that has been claimed to be implicated in oxide ion mobility.

Acknowledgements

Funding is gratefully acknowledged from the Australian Research Council. BMG acknowledges the support from the Australian Institute of Nuclear Science and Engineering. We also thank ANSTO's Australian Centre for Neutron Scattering for instrument time on Wombat DB9101. This research was facilitated by access to Sydney Analytical, a core research facility at the University of Sydney.

References

1. Clarke, D. R.; Oechsner, M.; Padture, N. P., Thermal-barrier coatings for more efficient gas-turbine engines. *Mrs Bulletin* **2012,** *37* (10), 891-902.
2. Haugsrud, R.; Norby, T., Proton conduction in rare-earth ortho-niobates and ortho-tantalates. *Nature Materials* **2006,** *5* (3), 193-196.
3. de los Reyes, M.; Aughterson, R. D.; Gregg, D. J.; Middleburgh, S. C.; Zaluzec, N. J.; Huai, P.; Ren, C.; Lumpkin, G. R., Ion beam irradiation of ABO_4 compounds with the fergusonite, monazite, scheelite, and zircon structures. **2020,** *103* (10), 5502-5514.
4. Faure, N.; Borel, C.; Couchaud, M.; Basset, G.; Templier, R.; Wyon, C., Optical properties and laser performance of neodymium doped scheelites $CaWO_4$ and $NaGd(WO_4)_2$. *Applied Physics B-Lasers and Optics* **1996,** *63* (6), 593-598.
5. Ning, K.; Zhang, Q.; Zhang, D.; Fan, J.; Sun, D.; Wang, X.; Hang, Y., Crystal growth, characterization of $NdTaO_4$: A new promising stoichiometric neodymium laser material. *Journal of Crystal Growth* **2014,** *388*, 83-86.
6. Yang, X. Y.; Fernandez-Carrion, A. J.; Wang, J. H.; Porcher, F.; Fayon, F.; Allix, M.; Kuang, X. J., Cooperative mechanisms of oxygen vacancy stabilization and migration in the isolated tetrahedral anion Scheelite structure. *Nature Communications* **2018,** *9*.
7. Kendrick, E.; Kendrick, J.; Knight, K. S.; Islam, M. S.; Slater, P. R., Cooperative mechanisms of fast-ion conduction in gallium-based oxides with tetrahedral moieties. *Nature Materials* **2007,** *6* (11), 871-875.
8. Rooksby, H. P.; White, E. A. D., Structures of 1:1 compounds of rare earth oxides with niobia and tantala. *Acta Crystallographica* **1963,** *16* (9), 888-890.
9. Brixner, L. H.; Chen, H. Y., On the structural and luminescent properties of the $M'LnTaO_4$ rare-earth tantalates. *Journal of the Electrochemical Society* **1983,** *130* (12), 2435-2443.

10. Keller, C., Uber ternare oxide des niobs und tantals vom typ ABO_4. *Zeitschrift Fur Anorganische Und Allgemeine Chemie* **1962,** *318* (1-2), 89-106.
11. Santoro, A.; Marezio, M.; Roth, R. S.; Minor, D., Neutron powder diffraction study of the structures of $CeTaO_4$, $CeNbO_4$, and $NdTaO_4$. *J. Solid State Chem.* **1980,** *35* (2), 167-175.
12. Tsunekawa, S.; Kamiyama, T.; Sasaki, K.; Asano, H.; Fukuda, T., Precise structure-analysis by neutron-diffraction for $RNbO_4$ and distortion of NbO_4 tetrahedra. *Acta Crystallogr. Sect. A* **1993,** *49*, 595-600.
13. Stubican, V. S., High temperature transitions in rare-earth niobates and tantalates. *Journal of the American Ceramic Society* **1964,** *47* (2), 55-58.
14. Siqueira, K. P. F.; Dias, A., Effect of the processing parameters on the crystalline structure of lanthanide orthotantalates *J Materials Research* **2014,** *17*, 167-173.
15. Titov, Y. A.; Sych, A. M.; Sokolov, A. N.; Kapshuk, A. A.; Markiv, V. Y.; Belyavina, N. M., Crystal structure of the high-pressure modification of $NdTaO_4$. *Journal of Alloys and Compounds* **2000,** *311* (2), 252-255.
16. Arulnesan, S. W.; Kayser, P.; Kimpton, J. A.; Kennedy, B. J., Studies of the fergusonite to scheelite phase transition in $LnNbO_4$ orthoniobates. *J. Solid State Chem.* **2019,** *277*, 229-239.
17. Shannon, R. D., Revised effective ionic-radii and systematic studies of interatomic distances in halides and chalcogenides. *Acta Crystallogr. Sect. A* **1976,** *32* (SEP1), 751-767.
18. Brixner, L. H.; Whitney, J. F.; Zumsteg, F. C.; Jones, G. A., Ferroelasticity in *Ln*NbO_4 type rare-earth niobates. *Mater. Res. Bull.* **1977,** *12* (1), 17-24.
19. Tsunekawa, S.; Takei, H., Domain switching behavior of ferroelastic $LaNbO_4$ and $NdNbO_4$. *Journal of the Physical Society of Japan* **1976,** *40* (5), 1523-1524.
20. Pellicer-Porres, J.; Garg, A. B.; Vázquez-Socorro, D.; Martínez-García, D.; Popescu, C.; Errandonea, D., Stability of the fergusonite phase in $GdNbO_4$ by high pressure XRD and Raman experiments. *J. Solid State Chem.* **2017,** *251*, 14-18.
21. Mariathasan, J. W. E.; Finger, L. W.; Hazen, R. M., High-pressure behavior of $LaNbO_4$. *Acta Crystallographica Section B* **1985,** *41* (3), 179-184.
22. David, W. I. F., The high-temperature paraelastic structure of $LaNbO_4$. *Mater. Res. Bull.* **1983,** *18* (6), 749-756.
23. Takei, H.; Tsunekawa, S., Growth and properties of $LaNbO_4$ and $NdNbO_4$ single-crystals. *Journal of Crystal Growth* **1977,** *38* (1), 55-60.
24. Jian, L.; Wayman, C. M., Monoclinic-to-tetragonal phase transformation in a ceramic rare-earth orthoniobate, $LaNbO_4$. *Journal of the American Ceramic Society* **1997,** *80* (3), 803-806.
25. Huse, M.; Skilbred, A. W. B.; Karlsson, M.; Eriksson, S. G.; Norby, T.; Haugsrud, R.; Knee, C. S., Neutron diffraction study of the monoclinic to tetragonal structural transition in $LaNbO_4$ and its relation to proton mobility. *J. Solid State Chem.* **2012,** *187*, 27-34.
26. Sarin, P.; Hughes, R. W.; Lowry, D. R.; Apostolov, Z. D.; Kriven, W. M., High-Temperature Properties and Ferroelastic Phase Transitions in Rare-Earth Niobates ($LnNbO_4$). *Journal of the American Ceramic Society* **2014,** *97* (10), 3307-3319.
27. Brunckova, H.; Mudra, E.; Medvecky, L.; Kovalcikova, A.; Durisin, J.; Sebek, M.; Girman, V., Effect of lanthanides on phase transformation and structural properties of $LnNbO_4$ and $LnTaO_4$ thin films. *Materials & Design* **2017,** *134*, 455-468.
28. Shian, S.; Sarin, P.; Gurak, M.; Baram, M.; Kriven, W. M.; Clarke, D. R., The tetragonal-monoclinic, ferroelastic transformation in yttrium tantalate and effect of zirconia alloying. *Acta Materialia* **2014,** *69*, 196-202.
29. Studer, A. J.; Hagen, M. E.; Noakes, T. J., Wombat: The high-intensity powder diffractometer at the OPAL reactor. *Physica B-Condensed Matter* **2006,** *385-86*, 1013-1015.
30. Larson, A. C.; Von Dreele, R. B., General Structure Analysis System (GSAS). **1994**.
31. Toby, B. H., EXPGUI, a graphical user interface for GSAS. *J. Appl. Cryst.* **2001,** *34*, 210-213.
32. Momma, K.; Izumi, F., VESTA 3 for three-dimensional visualization of crystal, volumetric and morphology data. *J. Appl. Crystallogr.* **2011,** *44*, 1272-1276.

33. Brese, N. E.; Okeeffe, M., Bond valence parameters for solids. *Acta Crystallographica Section B-Structural Science* **1991,** *47*, 192-197.
34. Brown, I. D., Recent Developments in the Methods and Applications of the Bond Valence Model. *Chemical Reviews* **2009,** *109* (12), 6858-6919.
35. Chay, C.; Avdeev, M.; Brand, H. E. A.; Injac, S.; Whittle, T. A.; Kennedy, B. J., Crystal structures and phase transition behaviour in the 5d transition metal oxides $AReO_4$ (A = Ag, Na, K, Rb, Cs and Tl). *Dalton Transactions* **2019,** *48* (47), 17524-17532.
36. Injac, S.; Yuen, A. K. L.; Avdeev, M.; Wang, C. H.; Turner, P.; Brand, H. E. A.; Kennedy, B. J., Structural and Magnetic Studies of ABO_4 Type Ruthenium and Osmium Oxides. *Inorganic Chemistry* **2020,** *59* (5), 2791-2802.
37. Kennedy, B. J.; Injac, S.; Thorogood, G. J.; Brand, H. E. A.; Poineau, F., Structures and Phase Transitions in Pertechnetates. *Inorganic Chemistry* **2019,** *58* (15), 10119-10128.
38. Tsunekawa, S.; Kamiyama, T.; Asano, H.; Fukuda, T., Relationship between covalence and displacive phase-transition temperature in RAO_4 and $LaAO_3$ (R=rare-earth element and A=Nb and Ta). *J. Solid State Chem.* **1995,** *116* (1), 28-32.
39. Brown, I. D.; Dabkowski, A.; McCleary, A., Thermal Expansion of Chemical Bonds. *Acta Crystallographica Section B* **1997,** *53* (5), 750-761.
40. Jacquet, Q.; Rousse, G.; Iadecola, A.; Saubanère, M.; Doublet, M.-L.; Tarascon, J.-M., Electrostatic Interactions versus Second Order Jahn–Teller Distortion as the Source of Structural Diversity in Li_3MO_4 Compounds (M = Ru, Nb, Sb and Ta). *Chemistry of Materials* **2018,** *30* (2), 392-402.
41. Mullens, B. G.; Avdeev, M.; Brand, H. E. A.; Mondal, S.; Vaitheeswaran, G.; Kennedy, B. J., Insights into the structural variations in $SmNb_{1-x}Ta_xO_4$ and $HoNb_{1-x}Ta_xO_4$ combined experimental and computational studies. *Dalton Transactions* **2021,** *50* (26), 9103-9117.
42. Shimakawa, Y.; Kubo, Y.; Tauchi, Y.; Kamiyama, T.; Asano, H.; Izumi, F., Structural distortion and ferroelectric properties of $SrBi_2(Ta_{1-x}Nb_x)_2O_9$. **2000,** *77* (17), 2749-2751.
43. Errandonea, D., Landau theory applied to phase transitions in calcium orthotungstate and isostructural compounds. *Europhysics Letters (EPL)* **2007,** *77* (5), 56001.
44. Carpenter, M. A.; Salje, E. K. H.; Graeme-Barber, A., Spontaneous strain as a determinant of thermodynamic properties for phase transitions in minerals. *European Journal of Mineralogy* **1998,** *10* (4), 621-691.
45. Hayward, S. A.; Salje, E. K. H., Cubic-tetragonal phase transition in $SrTiO_3$ revisited: Landau theory and transition mechanism. *Phase Transitions* **1999,** *68* (3), 501-522.
46. Aizu, K., Determination of state parameters and formulation of spontaneous strain for ferroelastics. *Journal of the Physical Society of Japan* **1970,** *28* (3), 706-&.
47. Schlenker, J. L.; Gibbs, G. V.; Boisen, M. B., Strain-tensor components expressed in terms of lattice-parameters. *Acta Crystallogr. Sect. A* **1978,** *34* (JAN), 52-54.
48. Perez-Mato, J. M.; Orobengoa, D.; Aroyo, M. I., Mode crystallography of distorted structures. *Acta Crystallogr. Sect. A* **2010,** *66* (5), 558-590.
49. Auckett, J. E.; Lopez-Odriozola, L.; Clark, S. J.; Evans, I. R., Exploring the nature of the fergusonite-scheelite phase transition and ionic conductivity enhancement by Mo^{6+} doping in $LaNbO_4$. *Journal of Materials Chemistry A* **2021,** *9* (7), 4091-4102.
50. Howard, C. J.; Knight, K. S.; Kennedy, B. J.; Kisi, E. H., The structural phase transitions in strontium zirconate revisited. *Journal of Physics: Condensed Matter* **2000,** *12* (45), L677-L683.
51. Ferrara, C.; Mancini, A.; Ritter, C.; Malavasi, L.; Tealdi, C., Interstitial oxide ion migration in scheelite-type electrolytes: a combined neutron diffraction and computational study. *Journal of Materials Chemistry A* **2015,** *3* (44), 22258-22265.